HYDROLOGICAL PROCESSES
Hydrol. Process. (2012)
Published online in Wiley Online Library
(wileyonlinelibrary.com) DOI: 10.1002/hyp.9514

Coupling of a simultaneous heat and water model with a distributed hydrological model and evaluation of the combined model in a cold region watershed

Yanlin Zhang,[1]* Guodong Cheng,[1] Xin Li,[1] Xujun Han,[1] Lei Wang,[2,3] Hongyi Li,[1] Xiaoli Chang[1] and G. N. Flerchinger[4]

[1] *Cold and Arid Regions Environmental and Engineering Research Institute, Chinese Academy of Sciences, Lanzhou, Gansu 730000, PR China*
[2] *Key Laboratory of Tibetan Environment Changes and Land Surface Processes, Institute of Tibetan Plateau Research, Chinese Academy of Sciences, Beijing, 100101, PR China*
[3] *Department of Civil Engineering, the University of Tokyo, Tokyo, Japan*
[4] *USDA Agricultural Research Service, Northwest Watershed Research Center, Boise, Idaho, USA*

Abstract:

Snow and frozen soil prevail in cold regions worldwide, and the integration of these processes is crucial in hydrological models. In this study, a combined model was developed by fully coupling a simultaneous heat and water model with a geomorphologically based distributed hydrological model. The combined model simulates vertical and lateral water transfer as well as vertical heat fluxes and is capable of representing the effects of frozen soil and snowmelt on hydrological processes in cold regions. This model was evaluated by using *in situ* observations in the Binggou watershed, an experimental watershed for cold region hydrology of the Watershed Allied Telemetry Experimental Research Project. Results showed that the model was able to predict soil freezing and thawing, unfrozen soil water content, and snow depth reasonably well. The simulated hydrograph was in good agreement with the *in situ* observation. The Nash–Sutcliffe coefficient of daily discharge was 0.744 for the entire simulation period, 0.472 from April to June, and 0.711 from June to November. This model can improve our understanding of hydrological processes in cold regions and assess the impacts of global warming on hydrological cycles and water resources. Copyright © 2012 John Wiley & Sons, Ltd.

KEY WORDS distributed hydrological model; frozen soil; snowmelt; cold region; Heihe River basin

Received 13 January 2012; Accepted 13 August 2012

INTRODUCTION

In winter, frozen soil occupies 55–60% of the land surface of the Northern Hemisphere (Zhang *et al*., 1999; Zhang *et al*., 2003a) and 72% of that in China (Li *et al*., 2008). Besides having a significant effect on soil heat and water fluxes, such conditions play an important role in hydrological and ecological processes in cold environments. The water phase transition in freezing/thawing cycles significantly alters soil water potential, which influences water evapouration and redistribution in the soil (Konrad and Duquennoi, 1993; Stahli *et al*., 1999; Zhang *et al*., 2003b). The ice in frozen soil modulates hydraulic properties such as infiltration capacity and hydraulic conductivity and, in turn, influences soil water transfer (Lundin, 1990; Stahli *et al*., 1996; Stahli *et al*., 1999; Koren, 2006). The underlying impermeable frozen soil generally prevents rainfall and snowmelt from infiltrating into deep soil, which may influence runoff generation and groundwater recharge (Cherkauer and Lettenmaier, 1999; Nyberg *et al*., 2001; Slater *et al*., 2001; Bayard and Stahli, 2005; Bayard *et al*., 2005; Quinton and Carey, 2008; Woo *et al*., 2008). The total water content conserved in frozen soil is an important controlling factor of runoff generation in the thawing period (Stahli *et al*., 1999; Stahli *et al*., 2001; Wright *et al*., 2008). Runoff generation on hillslopes in cold regions is heavily influenced by the thawing depth of frozen soil, and its mechanisms differ from those in temperate regions. Both lateral and vertical soil water fluxes in cold regions are strongly dependent on soil freezing or thawing depths (Hayashi *et al*., 2007; Quinton and Carey, 2008). Therefore, detailed descriptions of frozen soil in hydrological models are indispensable for runoff prediction in cold regions (Takata, 2002; Hall *et al*., 2003; Luo *et al*., 2003). Models excluding frozen soil modules tend to underestimate snowmelt runoff and accumulated discharge (Stahli *et al*., 2001; Pohl *et al*., 2005). In the Northern Hemisphere, many rivers originate from highlands and mountainous regions where the soil is exposed to freezing temperatures. In the context of global warming, permafrost tends to degrade, and the penetration depth of seasonal frozen soil changes. Consequently, water resource availability and annual distribution are affected. Therefore, hydrological models that consider frozen soil are necessary for integrated water resource management.

Numerous frozen soil parameterisation schemes have been developed and tested (Harlan, 1973; Jansson and Halldin, 1979; Flerchinger and Saxton, 1989; Stahli *et al*., 1996;

*Correspondence to: Yanlin Zhang, Laboratory of Remote Sensing and Geospatial Science, Cold and Arid Regions Environmental and Engineering Research Institute, Chinese Academy of Sciences, Lanzhou, Gansu 730000, PR China.
E-mail: yanlinzhang@lzb.ac.cn

Koren *et al.*, 1999; Jansson and Moon, 2001; Woo *et al.*, 2004; Koren, 2006; Li *et al.*, 2009a; Li *et al.*, 2010). Several have been incorporated into land surface models, such as the simple biosphere model version 2 (SiB2), the community/common land model, and the variable infiltration capacity (VIC) model (Cherkauer and Lettenmaier, 1999; Slater *et al.*, 2001; Cherkauer and Lettenmaier, 2003; Li and Koike, 2003; Niu and Yang, 2006; Yi *et al.*, 2006). In addition, frozen soil processes have been considered in distributed hydrological models such as the water and energy budget-based distributed hydrological model (WEB-DHM) (Wang *et al.*, 2010), the GEOtop model (Rigon *et al.*, 2006), the arctic hydrological and thermal process model (Zhang *et al.*, 2000), the cold region hydrological model (Pomeroy et al., 2007), the distributed water heat coupled model (Chen *et al.*, 2008), and others (Stahli *et al.*, 1996; Stahli *et al.*, 2001; Rawlins *et al.*, 2003; Yamazaki *et al.*, 2006). However, with the exception of VIC and GEOtop, most frozen soil schemes in hydrological models are simplified and empirical. Although some empirical schemes are capable of estimating the depth of soil freezing and thawing, they rarely simulate soil temperature and ice content or their influences on heat and water fluxes. Moreover, these schemes usually involve empirical parameters or formulae that must be calibrated for specific regions that vary with time (Stahli *et al.*, 1999). VIC is designed for large scales from continental river basins to the entire globe, with spatial resolutions ranging from 1/8° to 2° (Liang *et al.*, 1994; Cherkauer and Lettenmaier, 1999). On the contrary, GEOtop, which features three-dimensional soil water flux and one-dimensional energy balance, is designed for simulation in small watersheds with high spatial resolution (http://www.geotop.org/cgi-bin/moin.cgi). When applied to a large basin, the computational cost increases significantly. The efficient framework of WEB-DHM makes it practical for large basins. However, its frozen soil parameterisation is simple and empirical. Distributed hydrological models with physically based frozen soil modules remain in research.

The focus of this study is to couple a one-dimensional simultaneous heat and water model (SHAW) (Flerchinger and Saxton, 1989) with a geomorphologically based distributed hydrological model (GBHM) (Yang, 1998). The coupled model, SHAWDHM, addresses vertical heat and water fluxes in the soil vegetation atmosphere transfer (SVAT) system and lateral water flow on hillslopes. With this model, the impacts of vegetation, residue, topography, snow, and atmospheric conditions on soil freezing/thawing, and their influences on hydrological processes in cold regions can be fully considered. The coupled model was evaluated in the Binggou watershed, a small experimental watershed used for cold region hydrology studies in the Watershed Allied Telemetry Experimental Research (WATER) Project (Li *et al.*, 2009b). This paper includes a review of relevant models and a description of the coupled model development in section 2. Background information of the study area and datasets are presented in section 3, and the results and conclusions are presented in sections 4 and 5, respectively.

MODEL DESCRIPTION

Review of relevant models

The GBHM, originally developed (Yang, 1998; Yang *et al.*, 2002) and further modified into grid-based style by Yang *et al.* (2004), employed hillslope as the basic hydrologic response unit. A sub-grid parameterisation method was used to consolidate the topographic information of a model grid into hillslopes on the basis of finer digital elevation model (DEM), which increases model efficiency when used in large watersheds. Essentially, the structure of hillslopes connected by a river network embodied in the model physically represents the spatial patterns of hydrological processes in a watershed. Wang *et al.* (2009a, b) coupled the GBHM with the three-layered Sib2. This coupled model, WEB-DHM, assimilated advantages from the physically based land surface model and improved the prediction of water and energy fluxes on a hillslope and stream discharge (Wang *et al.*, 2009b; Jaranilla-Sanchez *et al.*, 2011). Subsequently, the WEB-DHM was further improved by incorporating an empirical frozen soil module (Wang *et al.*, 2010).

On the other hand, the SHAW model was designed to simulate soil freezing and thawing cycles. With more than 20 years in development, this model fully addresses the hydrological and thermal processes in a one-dimensional vertical profile extending either from the top of canopy, snow, or residue or from the soil surface to a specified soil depth (Flerchinger and Saxton, 1989). SHAW has an excellent record in simulating heat and water fluxes in the SVAT system in cold regions. The physical processes are governed by a set of partial differential equations that were solved simultaneously by the finite difference method. A discrete layered system was established to describe liquid, vapour, heat, and solute fluxes. This model can estimate soil freezing or thawing depth, temperatures, soil water and ice content, and solute concentration, as well as snow accumulation and ablation. Therefore, the SHAW model was selected for coupling with a distributed hydrological model because of its excellent performance in describing snow and frozen soil processes in cold regions.

Model development

The SHAW and GBHM were fully coupled under the framework of the grid-based GBHM (Yang *et al.*, 2004; Wang *et al.*, 2009a). The structure and lateral hydrological processes of GBHM were retained as a hydrological sub-model, whereas its vertical processes such as canopy interception, snowmelt, infiltration, and soil water transfer were replaced by those of SHAW. The hydrological sub-model and SHAW shared the same layered system, which includes vertical discretisation and state variables such as soil water content, ice content, and hydraulic conductivity. The coupled model, SHAWDHM, describes frozen soil processes and its relationship with snowmelt, infiltration, evapouration, and runoff generation in a physically based method to simulate the hydrological processes in cold regions.

DOI: 10.1002/hyp

In this section, the SHAWDHM is described in detail, as illustrated in Figure 1. The method for catchment discretisation is introduced, and a watershed is discretised into spatially distributed model grids. The topography of these grids is assumed to comprise homogeneous hillslopes on which GBHM and SHAW are coupled. The model components and the coupling strategy are subsequently detailed.

Catchment discretisation. The catchment discretisation was inherited from the grid-based GBHM. As shown in Figure 1 a), a watershed was first divided into nine sub-basins based on the DEM by using the method proposed by Pfafstetter. Each sub-basin can also be divided into nine (Pfafstetter, 1989; Verdin and Verdin, 1999). This recursive subdivision procedure had a maximum level of three; that is, a watershed can be divided into a maximum of 729 sub-basins. In each sub-basin, a series of flow intervals can be identified according to the flow distance to its outlet. This sub-basin and flow interval structure simplified the river routing procedure. Flow intervals were further divided into several model grids. Thus, the entire watershed was tiled by spatially distributed model grids. The topography in a model grid was assumed to be hillslopes located along channels, as shown in Figure 1 b). Provided that the total river network length in a model grid extracted from finer DEM is $\sum L$, the topography in the model grid can be consolidated as a couple of geometrically symmetrical hillslopes of length $l=A/2\sum L$ along the river, where A is the grid area (m^2). In these virtual hillslopes, the canopy, residue, snow, and soil were divided into multiple layers parallel to the slope. The vertical heat and water fluxes and lateral water flows such as overland flow, interflow, and baseflow were simulated in the layered system.

Model components and model coupling. The same layered system as that for hillslopes was adopted for SHAW and GBHM, and they were coupled by sharing the same set of variables such as liquid soil water content, ice content, and soil hydraulic properties. In each time step, vertical heat and water fluxes, lateral water flows, and river routing were simulated in a coupled way. The model components and coupling strategy are described in detail as follows.

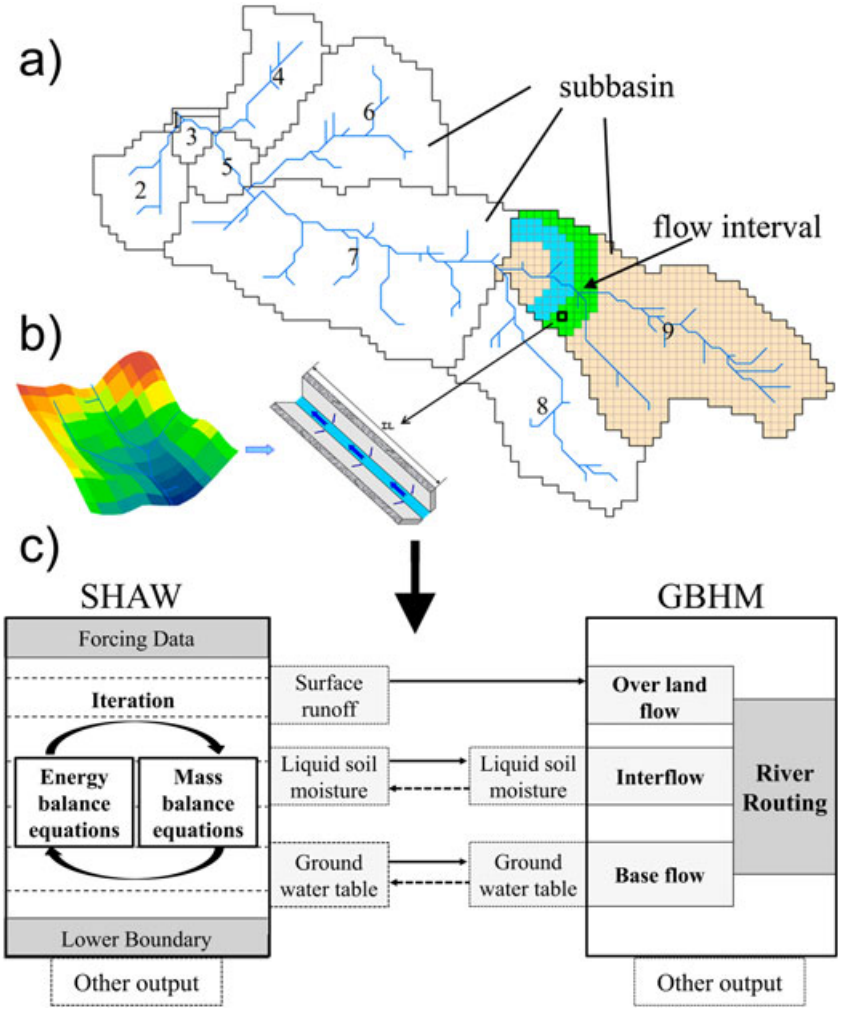

Figure 1. Overall structure of the coupled simultaneous heat and water distributed hydrological model (SHAWDHM). a) Catchment discretisation. The watershed is divided into nine sub-basins, denoted, respectively, as 1–9. Each sub-basin can be recursively divided into sub-basins that are further subdivided into flow interval and composed of several model grids; b) consolidation of topographic information from a model grid into hillslopes by using sub-grid parameterisation; c) coupling of SHAW and GBHM on hillslopes in every model grid

DOI: 10.1002/hyp

Step 1. Vertical heat and water fluxes. The SHAW model was initially run on the hillslopes. One-dimensional vertical heat and water fluxes in the SVAT system were governed by coupled partial differential equations based on energy and mass conservation as follows (Flerchinger and Saxton, 1989):

$$C_s\frac{\partial T}{\partial t}-\rho_i L_f\frac{\partial \theta_i}{\partial t}=\frac{\partial}{\partial z}\left[k_s\frac{\partial T}{\partial z}\right]-\rho_l c_l\frac{\partial q_l T}{\partial z}-L_v\left(\frac{\partial q_v}{\partial z}-\frac{\partial \rho_v}{\partial t}\right)+R_n \quad (1)$$

$$\frac{\partial \theta_l}{\partial t}+\frac{\rho_i}{\rho_l}\frac{\partial \theta_i}{\partial t}=\frac{\partial}{\partial z}\left[K\left(\frac{\partial \psi}{\partial z}+1\right)\right]+\frac{1}{\rho_l}\frac{\partial q_v}{\partial z}+U \quad (2)$$

The relationships between the soil matric potential (ψ), liquid soil water content (θ_l), hydraulic conductivity (K), and soil temperature (T) can be established by the following equations (Clapp and Hornberger, 1978; Fuchs *et al.*, 1978):

$$\psi=\psi_e\left(\frac{\theta_l}{\theta_s}\right)^{-b} \quad (3)$$

$$K=K_s\left(\frac{\theta_l}{\theta_s}\right)^{2b+3} \quad (4)$$

$$\psi=\frac{L_f}{g}\left(\frac{T}{T_K}\right) \quad (5)$$

where C_s is the volumetric heat capacity of soil ($\mathrm{Jm^{-3}\,^\circ C^{-1}}$); T is the soil temperature (°C); t is time (s); ρ_i is the density of ice ($\mathrm{kg\,m^{-3}}$), and L_f is its latent heat of fusion (335,000 $\mathrm{Jkg^{-1}}$); θ_i is the volumetric ice content of soil; k_s is the thermal conductivity of soil ($\mathrm{Wm^{-1}C^{-1}}$); z is the vertical distance from the surface (m); ρ_l is the density of liquid water, and c_l is its specific heat capacity ($\mathrm{Jm^{-3}C^{-1}}$); q_l is the liquid water flux ($\mathrm{ms^{-1}}$); q_v is the vapour water flux ($\mathrm{kgm^{-2}\,s^{-1}}$); L_v is the latent heat of vapourisation of water ($\mathrm{Jkg^{-1}}$); ρ_v is the vapour density of water ($\mathrm{kgm^{-3}}$); R_n is the net downward radiation flux incident on the soil surface ($\mathrm{Wm^{-2}}$); θ_l is the volumetric liquid water content of soil; K is the hydraulic conductivity of unsaturated soil ($\mathrm{ms^{-1}}$); ψ is the soil water potential (m); U is a source/sink term for water flux ($\mathrm{m^3m^{-3}\,s^{-1}}$); ψ_e is the air-entry potential of soil (m); K_s is the hydraulic conductivity of saturated soil ($\mathrm{ms^{-1}}$); b is the soil pore size distribution parameter; g is the acceleration of gravity (9.81 $\mathrm{m\,s^{-2}}$); and T_k is the absolute soil temperature (K).The coupled partial differential equations were discretised into implicit finite difference form and were solved by using the Newton Raphson iteration technique. As a result, vertical heat and water fluxes can be estimated in addition to state variables in the SVAT system, including temperature, liquid water content, water vapour density, ice content, snow depth, snowmelt, infiltration, surface runoff, and surface water ponding. Moreover, the hydraulic conductivities of each soil layer were updated, and a simple groundwater aquifer node was added below the soil layers. Interactions between the groundwater and unsaturated zone were simulated by using Darcy's law.

Step 2. Overland flow. In step 1, the infiltration excess was calculated by using the Green–Ampt equation (Green and Ampt, 1911; Flerchinger, 2000), and surface water storage h (m) was maintained. Overland flow along the hillslope surface was governed by Manning's steady sheet flow. After overland flow calculation, surface water storage was updated and used as the upper boundary condition of the vertical water transfer problem in the next time step:

$$\frac{\partial h}{\partial t}+\frac{\partial q_s}{\partial l}=i \qquad q_s=\frac{1}{n}S_0^{1/2}h^{5/3} \quad (6)$$

where q_s is the overland flow per unit width ($\mathrm{m^3s^{-1}\,m^{-1}}$); h is the water storage depth (m); t is time (s); l is the distance along the hill slope (m); i is the net input rate (m/s); S_0 is the hill slope gradient; and n is the Manning roughness parameter.

Step 3. Subsurface flow. The lateral subsurface flow in the unsaturated soil along hillslopes is driven by gravity forces when the liquid soil water content is higher than the field capacity:

$$\begin{cases} \mathrm{q_{sub1}}=\sum_{\mathrm{i}}^{\mathrm{N}}\mathrm{K_i}\Delta z_\mathrm{i}\sin\alpha & \text{if } \theta_{k_L}>\theta_f \\ \mathrm{q_{sub}}=\max(\mathrm{q_{sub1}},\Delta \mathrm{z_i}(\theta_{\mathrm{i_L}}\text{-}\theta_{\mathrm{f_L}})) \end{cases} \quad (7)$$

where q_{sub} is subsurface flow per unit width ($\mathrm{m^3s^{-1}\,m^{-1}}$); N is the number of soil layers; i is the soil layer index; $\alpha$is the slope; K_i is the hydraulic conductivity of *i-th* soil layer ($\mathrm{ms^{-1}}$); Δz_i is the thickness of *i-th* soil layer (m); θ_{il} is the volumetric liquid soil water content of *i-th* soil layer; and θ_{fl} is the volumetric field capacity of *i-th* soil layer.

Step 4. Baseflow. Interactions between groundwater and river were calculated by using Darcy's law. Hydraulic conductivity was adjusted according to the frozen depth of the aquifer. When the freezing front was deeper than the maximum soil depth prescribed in the model, Stefan's equation was employed to estimate the frozen depth of the aquifer by using the bottom layer temperature as the driving force:

$$q_g=K_g\left(1-\frac{D_f}{D_g}\right)\quad\frac{H_1-H_2}{L/2}\frac{h_1+h_2}{2} \quad (8)$$

where q_g is the baseflow per unit width ($\mathrm{m^3s^{-1}\,m^{-1}}$); K_g is the groundwater hydraulic conductivity ($\mathrm{m\,s^{-1}}$); L is the slope length (m); D_g is the thickness of the aquifer (m); and D_f is the frozen depth of aquifer (m). h_1, h_2, H_1, and H_2 are shown in Figure 2.

Step 5. River routine. A virtual channel was allocated for each flow interval. The channels were connected consecutively from upstream to downstream in the sub-basin to form a virtual river. Linked virtual rivers of all sub-basins comprised the virtual river network,

DOI: 10.1002/hyp

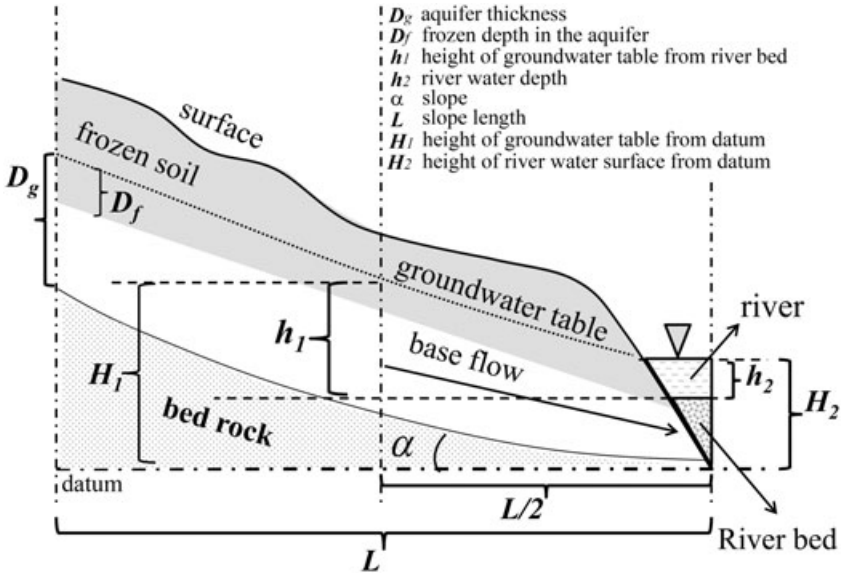

Figure 2. Interactions between groundwater and river

which accumulated the overland flow, subsurface flow, and baseflow from all grids. The runoff from each model grid entered the corresponding virtual channel and was routed through the network by using the kinematic approximation of the Saint Venant equations (Yang, 1998; Yang *et al*., 2002; Yang *et al*., 2004):

$$\frac{\partial Q}{\partial x} + \frac{\partial A}{\partial t} = q = q_s + q_{sub} + q_g \tag{9}$$

$$Q = \frac{1}{n} \frac{S_0^{1/2}}{p^{2/3}} \cdot A^{5/3} \tag{10}$$

where Q is the discharge at a given river section (m^3s^{-1}); x is the distance along the longitudinal axis of the river (m); A is the cross-sectional area (m^2); q is the lateral flux in each flow interval, including overland flow, subsurface flow, and baseflow (m^2s^{-1}); n is the Manning roughness; p is the wetted perimeter (m), i.e. the length of a line in contact with the water; t is time (s); and S_0 is the river bed slope.

Step 6. Return to Step 1 and repeat for next time interval.

MODEL EVALUATION

Study area

The coupled model was evaluated in the Binggou watershed (100°12′–100°18′E and 38°1′–38°4′N), which is an experimental watershed for cold region hydrology of the WATER Project (Li *et al*., 2009b). The watershed, located in the upper reaches of the Heihe River basin in northwest China, covers an area of 30.4 km^2 and is a high mountainous head watershed with elevations ranging from 3440 to 4400 m. The watershed is in a typical cold region where frozen soil is common. Observations from 1984 to 1991 indicate that the long-term average annual air temperature was approximately −2.5 °C at an altitude of 3,450 m, and the minimum air temperature reached −30.8 °C (Yang *et al*., 1993). Both permafrost and seasonal frozen soil exist in the watershed. Regions higher than 4000 m are dominated by permafrost, whereas seasonally frozen soil is distributed in areas below 4000 m. The mean annual precipitation is approximately 686 mm. Snowfall prevails from October to April, accounting for approximately 30% of the total precipitation.

Datasets

Meteorological data. In the WATER project, two stations were installed in the watershed: Dadongshu Snow Observation Station (DY, at 100°14′E, 38°01′N; 4,146.8 m) and Binggou Station (BG, at 100°13′E, 38°04′N; 3,449.4 m); see Figure 3. The DY station was equipped with an automatic weather station and an ultrasonic snow depth sensor (SR50). Continuous meteorological forcing data, soil temperature and moisture, snow depth, and other fluxes were obtained from 1 November 2007 to 21 November 2008 (Li and Wang, 2011). At one of the automatic weather stations at BG, only the meteorological forcing data (without precipitation) and soil temperature from 14 March 2008 to 31 December 2009 were collected owing to battery malfunction.

Meteorological data measured at DY were used to derive hourly spatially distributed forcing data. Hourly meteorological series were first aggregated from the 10-min logged raw data at DY. Because of the lack of data, the relative humidity, precipitation, wind speed, and downward shortwave radiation in the watershed were assumed as spatially uniform, and values were taken from the DY station. This assumption is reasonable since the watershed is relatively small. When overlap existed in observing time between BG and DY, i.e. from 14 March 2008 to 21 November 2008, air temperatures in the watershed were interpolated against elevations based on

DOI: 10.1002/hyp

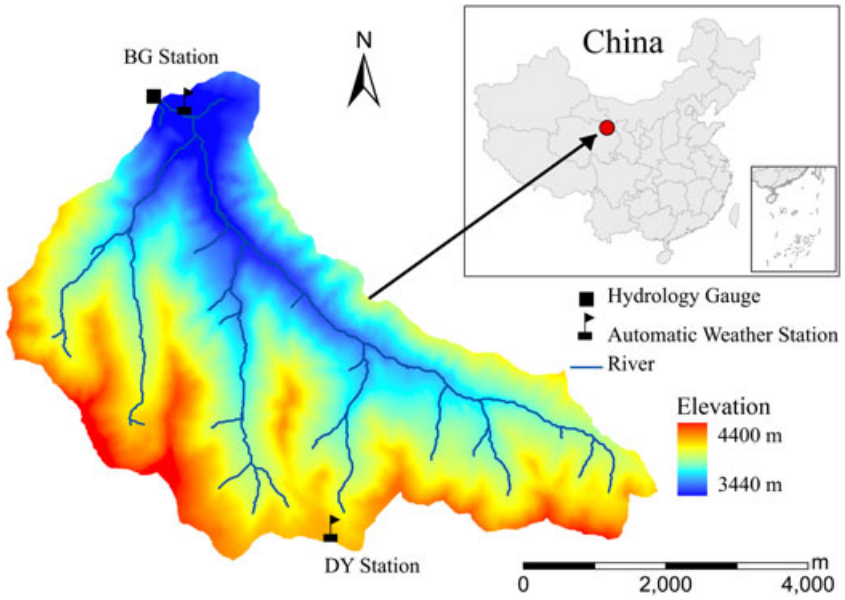

Figure 3. Schematic map of Binggou watershed

measurements at both stations. Average hourly air temperature lapse rates of all days from March to November, as well as those in months with observations, were calculated and sketched (Figure 4). The former was used to interpolate air temperatures against elevations in December, January, and February on the basis of DY observations. Note that the snowfall measured by rainfall gauge was significantly underestimated in winter and spring. A more realistic snowfall series was derived from observed snow depths. When air temperature was below the freezing point and the increase in snow depth per hour was greater than 2 cm, equivalent water corresponding to the snow depth increase was converted to precipitation. The required snow density was calculated as an empirical function of air temperature in the following equation, where T is the air temperature (°C) (Schmidt and Gluns, 1991; Hedstrom and Pomeroy, 1998; Pomeroy *et al.*, 1998). After the correction of snowfall in winter and spring, the total precipitation was 703 mm in the watershed.

$$\rho_{snowfall} = 67.9 + 51.3e^{T/2.6} \tag{11}$$

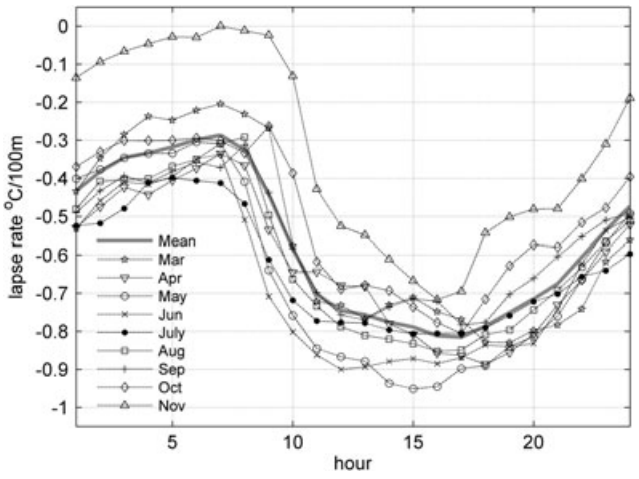

Figure 4. Mean hourly lapse rates of all days from March to November and those for months including observations

Vegetation and soil data. The dominant land cover type in the watershed is alpine meadow at altitudes of 3440–4000 m; the region above 4000 m is mainly alpine desert. The dynamic leaf area index (LAI) was obtained from 8-day composites (MOD15A2) of the Moderate Resolution Imaging Spectroradiometer that were interpolated into daily series. Because no dedicated soil surveys had been conducted in the region, the Harmonized World Soil Database (HWSD, http://www.iiasa.ac.at/Research/LUC/External-World-soil-database/HTML) was used to obtain the distributed soil properties. The soil map of China in the HWSD database was from the Second National Soil Survey of China (1995) conducted by the Institute of Soil Science of the Chinese Academy of Sciences (Shi *et al.*, 2004). In the database, soil columns were divided into two layers: a top layer (0–30 cm) and a sub-layer (30–100 cm). Physical soil properties include fractions of sand, silt, and clay; organic content; and bulk density. With these properties, the soil pore size distribution index, air-entry potential, and other hydraulic parameters required by the model were derived by using the method proposed by Saxton (Saxton and Rawls, 2006).

Model setup and calibration

The model adopted a spatial resolution of 250 m. The average soil depth was assumed to be 1.2 m in the watershed. Soil columns were divided into 11 layers, each of which was represented by one central node at 0, 0.05, 0.10, 0.15, 0.20, 0.30, 0.40, 0.60, 0.80, 1.00, and

DOI: 10.1002/hyp

1.20 m below the soil surface. The lower Dirichlet boundary condition of soil temperature was estimated by using the method proposed by Hirota *et al*. (2002), which required the mean annual temperature of deep soil (MAT, at 120 cm). The spatially distributed MATs were interpolated against elevations on the basis of observations made at DY with a mean lapse rate, which was calculated from observations at DY and BG to be approximately $-7\,\mathrm{K\,km^{-1}}$. For the water transfer problem, a unit gradient of soil water potential was assumed as the lower boundary condition.

The model was run in hourly steps from 20 November 2007 to 20 November 2008. Only point scale calibration was conducted at DY to obtain the dry soil albedo, canopy albedo, and residue albedo, which were 0.3, 0.24, and 0.3, respectively. Other parameters were assigned as those following either field observations or recommended values in the SHAW user manual. Owing to data limitations, several parameters, including roughness length for overland flow, momentum, and heat turbulence, were assumed as spatially uniform. Wang *et al*. (2010) conducted relevant works in the watershed with WEB-DHM, in which the same hydrological sub-model (i.e. GBHM) was used. Therefore, values for relevant parameters calibrated by Wang *et al*. (2010) were used in this study. These parameters included flow interval width, river width, river depth, Manning's coefficient, and riverbed slope. The initial distributed depth of groundwater table, snow depth, and soil water content were assigned according to the results of one-year spin-up period with forcing data from 20 November 2007 to 20 November 2008. The initial distributed soil temperatures were interpolated against elevations based on the soil temperature profile observed at DY on 20 November 2007.

RESULTS AND DISCUSSION

The root mean square error (RMSE) was used to quantitatively evaluate the model performance in simulating soil temperature and water content, and it was calculated as follows:

$$RMSE = \sqrt{\sum_{i=1}^{N} (y_{si}\text{-}y_{oi})^2 / N} \tag{12}$$

where y_{oi} is the observed series; y_{si} is the simulated series; and N is the number of observations. The Nash–Sutcliffe coefficient (NSE) was used to assess the performance in predicting stream discharge:

$$NSE = 1 - \frac{\sum_{i=1}^{N} (Q_{si} - Q_{oi})^2}{\sum_{i=1}^{N} (Q_{oi} - Q_{mo})^2} \tag{13}$$

here Q_{si} is the simulated discharge series; Q_{oi} is the observed series; and Q_{mo} is the mean of observed discharge. A high NSE indicates good model performance. An NSE value of 1 denotes a perfect match.

Snow pack and frozen soil evolutions

Figure 5 illustrates the spatial distribution of simulated snow depth and associated statistics. In general, snow began to accumulate in October or November in the watershed. At the beginning of accumulation, snow distribution was strongly related to topography because snowmelt was sensitive to air temperature. Higher regions with lower air temperatures enabled greater snow accumulation. In lower regions, higher or even positive

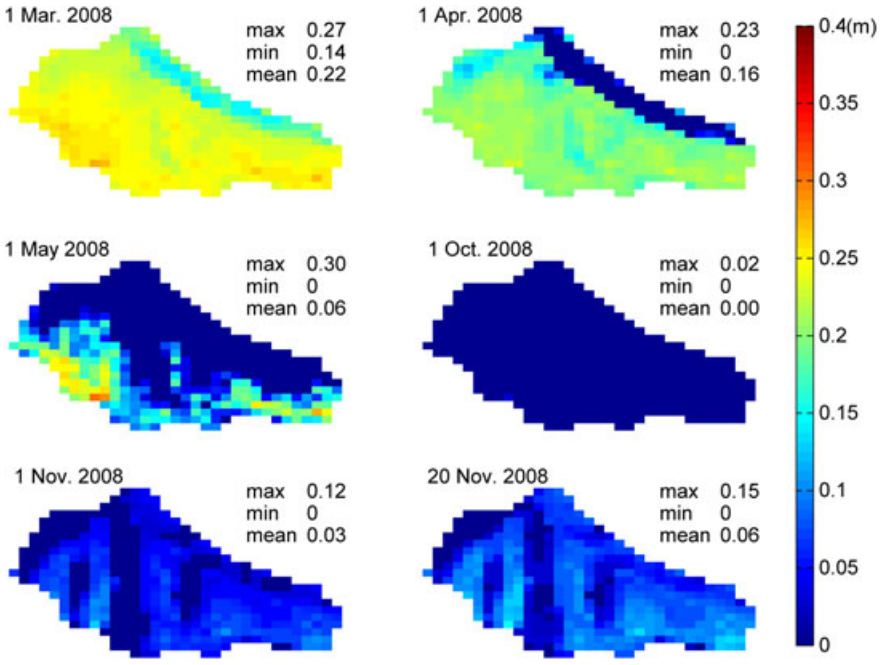

Figure 5. Spatial distribution of simulated snow depth and statistics on selected days in 2008

DOI: 10.1002/hyp

air temperatures resulted in rapid snowmelt. The snow in most regions reached maximum depths in February or March. However, snow distributions in March and April differed from that in November. They depended more on the total cumulative precipitation than on air temperature during winter and spring, since the air temperatures in winter were far below the freezing point, which was not beneficial to snowmelt. In March, snow in the lower regions began to melt and extended gradually to higher areas with increased air temperatures in April and May (Yang *et al.*, 1993). The snow cover usually disappeared in June in the watershed. However, significant snow accumulation of short duration occurred in some regions in early summer, which was confirmed by observation at DY (Figure 6).

The simulated and observed snow depths at DY from 21 November 2007 to 20 November 2008 are presented in Figure 6. Initially, the snow depth was in good agreement with the measurements when no significant snowfall occurred. However, from January onward, the simulated snow depth was occasionally underestimated. This may be attributed to the underestimated solid precipitation derived from the snow depth, as previously mentioned. Only an increase in snow depth greater than 2 cm per hour was identified as snowfall. Continuous light snowfall was ignored as noise when no significant snow depth increase per hour was observed. In addition, errors could be introduced by the empiric equation for snow density estimation because the equation was originally proposed for snowfall in forests. Regardless of the occasional discrepancies, however, the model yielded overall realistic snow depth prediction; RMSE was 0.033 m.

Figures 7 and 8 illustrate spatially distributed penetration depths of soil thawing and freezing fronts, respectively.

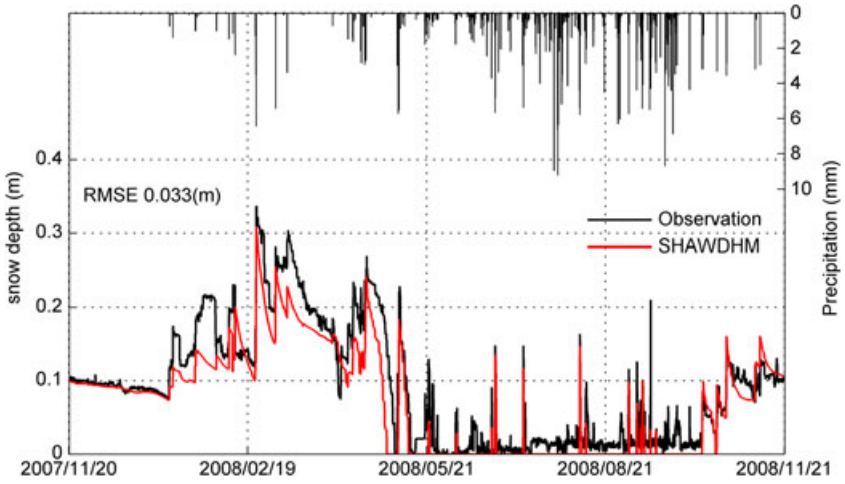

Figure 6. Hourly observed and simulated snow depths at DY from 21 November 2007 to 20 November 2008

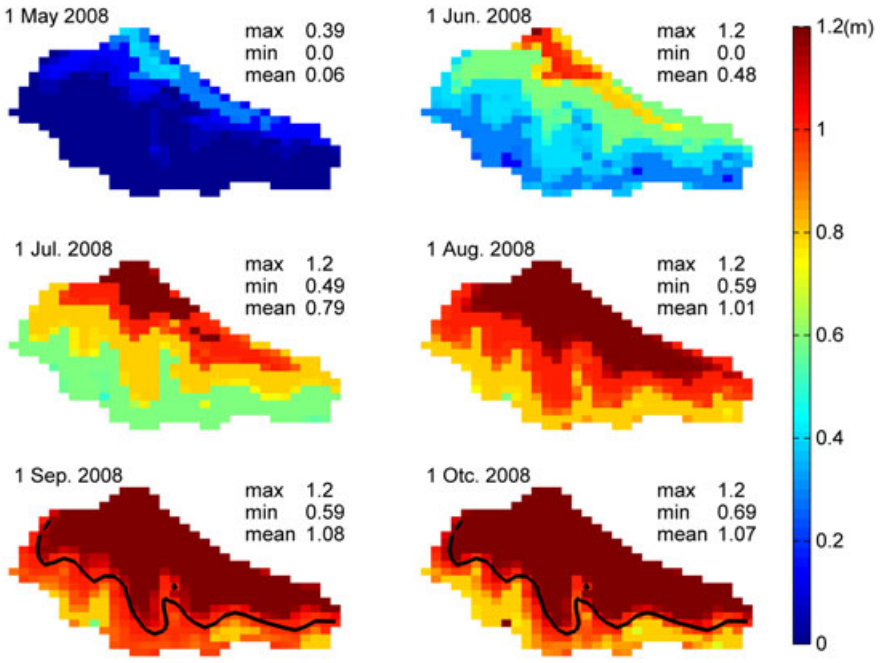

Figure 7. Simulated penetration depths of soil thawing front in the watershed on selected days in 2008. The black line represents the 4000 m contour line

DOI: 10.1002/hyp

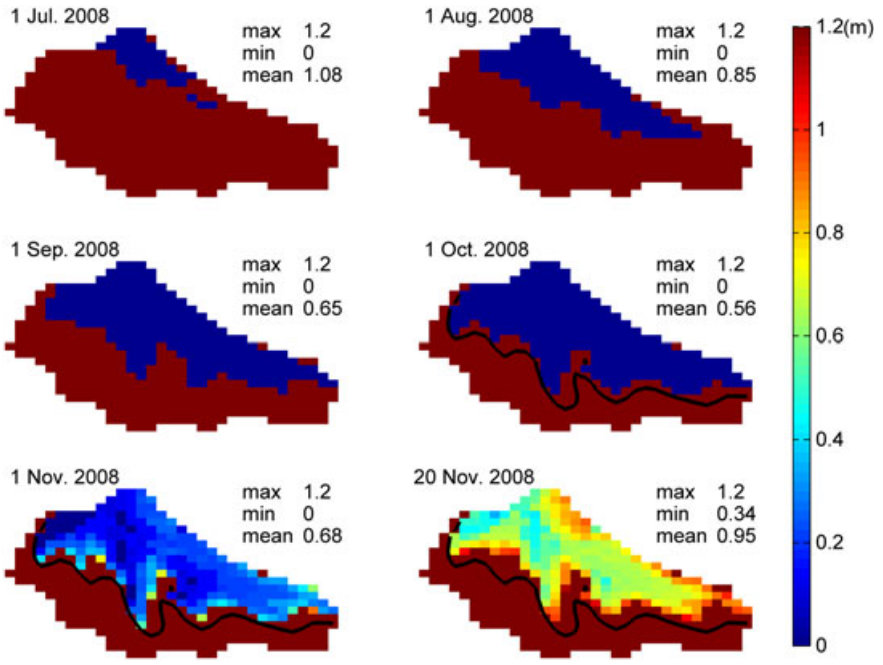

Figure 8. Simulated penetration depths of soil freezing front in the watershed on selected days in 2008. The black line represents the 4000 m contour line

Soil thawing began from the lower regions in late April and early May and progressed to ridge areas with an increase in air temperature. The thawing fronts reached maximum depths in mid-September, and the seasonal frozen soil melted completely. In late September, the soil began to refreeze. According to the survey by Yang *et al.* (1993), permafrost was distributed above 4000 m in the watershed, as indicated by black lines in Figures 7 and 8. The simulated seasonal frozen soil region is represented by the dark brown region in the lower right-hand panel of Figure 7; the other region is permafrost. These results are clearly consistent with Yang's survey. In addition, the observed soil thawing depths derived from the soil temperature profile and the simulated values at DY are compared in Figure 9. The frozen soil began to melt on 1 May. The melting was mainly constrained within the surface layer at approximately 0–25 cm. In June, the thawing front began to penetrate downward. In September,

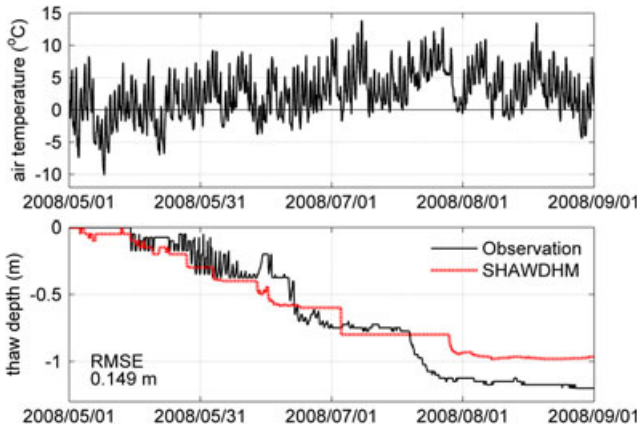

Figure 9. Hourly observed and simulated soil thawing depth derived from the temperature profile at DY from 1 May to 1 September 2008

the thawing process ceased, and the soil began to refreeze from the surface downward. The simulated maximum thawing depth was slightly underestimated at DY. This discrepancy may be attributed to the substantial thicknesses of soil layers prescribed in the model, which can cause inaccuracies in soil temperature simulation. The lower boundary condition of temperature could be an additional explanation. The simulated soil temperature at the lower boundary layer at 120 cm was slightly underestimated, as shown in Figure 10.

Soil temperature

Simulated soil temperatures at DY were compared with *in situ* observations (Figure 10). From February to March, the simulated soil temperatures near the surface (at 5, 10, and 20 cm) were obviously higher than the observed values when air temperature increased; the temperatures of deep soil were not affected by these warming events. These results may be attributed to underestimated snow depth (Figure 6), which did not provide adequate insulation from the warm air. Therefore, the soil warmed noticeably faster than observed temperatures. From March onward, the discrepancy between the simulated and observed temperatures began to diminish as the simulated snow depth became more consistent with measurements. From 7 April 2008, the observed soil temperatures increased nearly to the freezing point and decreased soon afterward. Large cracks may exist in the soil column, which allow warmer melt water from the surface to percolate rapidly into deep soil, providing a warming source. The soil temperatures decreased after refreezing of the melt water. The model failed to reproduce the soil temperatures of the top layers from September to November 2008. As shown in the top panels of Figure 10, simulated temperatures remained

DOI: 10.1002/hyp

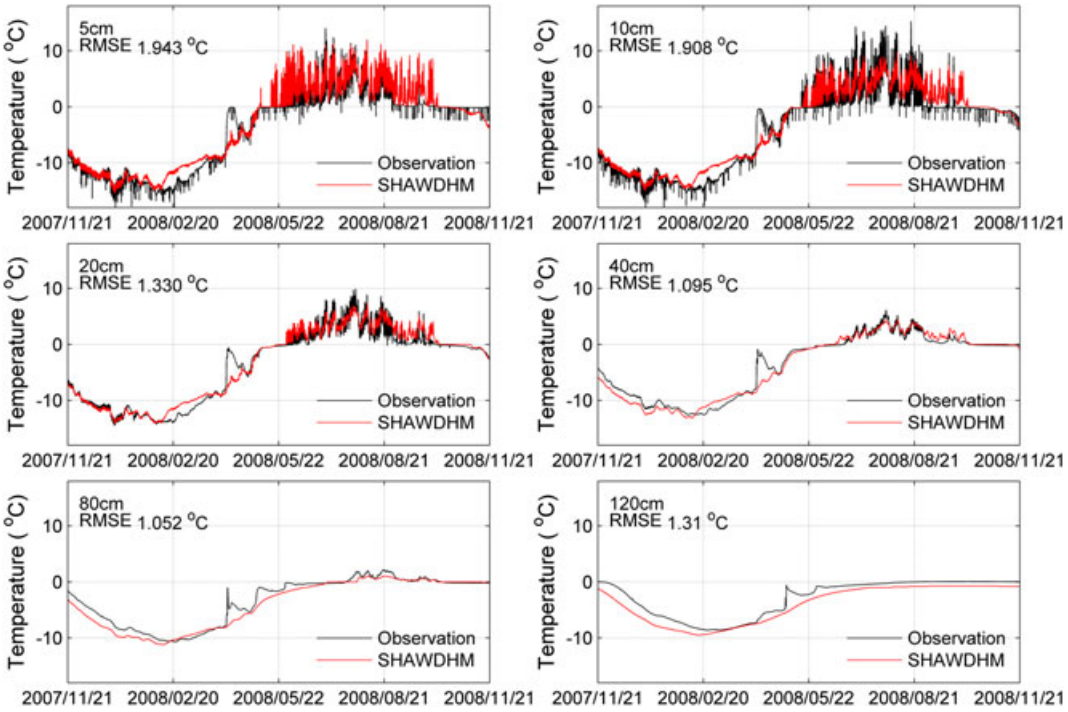

Figure 10. Hourly observed and simulated soil temperatures at several depths at DY from 21 November 2007 to 20 November 2008

positive for a lengthy period while the surface soil began to refreeze.

Figure 11 presents a comparison of simulated and observed soil temperatures at BG. The soil temperatures in summer were slightly underestimated, which may be attributed to the heterogeneity of vegetation and soil parameters such as LAI and thermal conductivity. Overall, the combined model reliably predicted soil temperatures in the watershed.

Liquid soil water content

Observation of liquid soil water content at BG was erroneous owing to sensor malfunction; therefore, only observations at DY were used to evaluate the model. Figure 12 presents a comparison between the observed and simulated volumetric liquid soil water content at DY. The surface soil began to melt on 15 May. However, the melting

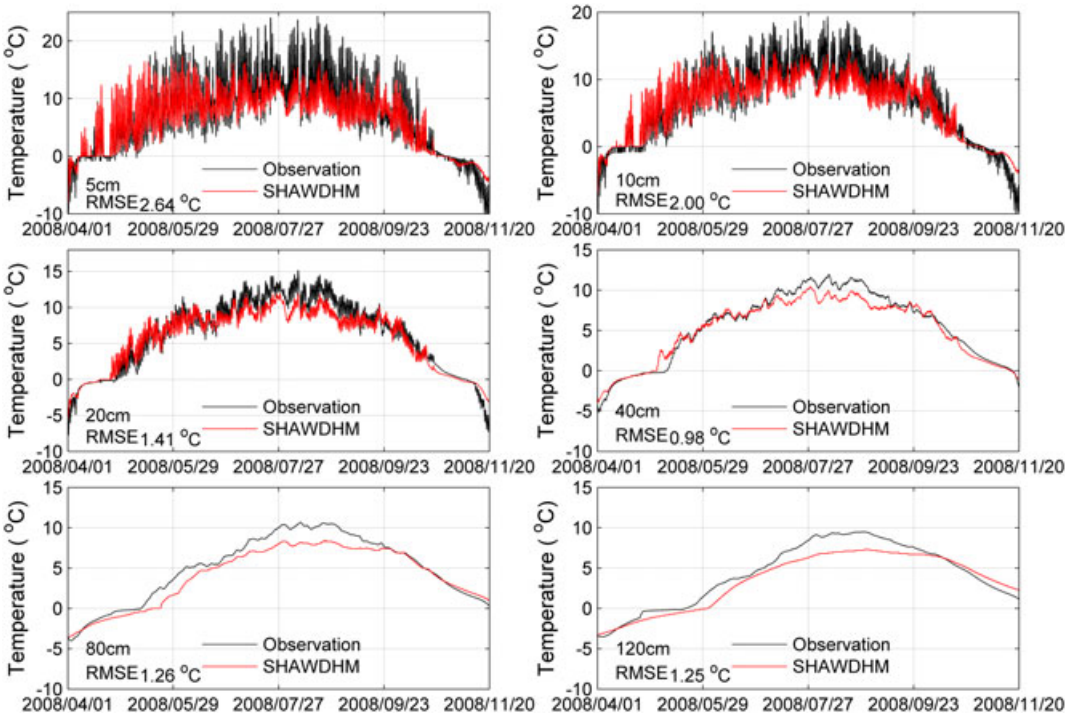

Figure 11. Hourly observed and simulated soil temperatures at several depths at BG from 1 April 2007 to 20 November 2008

DOI: 10.1002/hyp

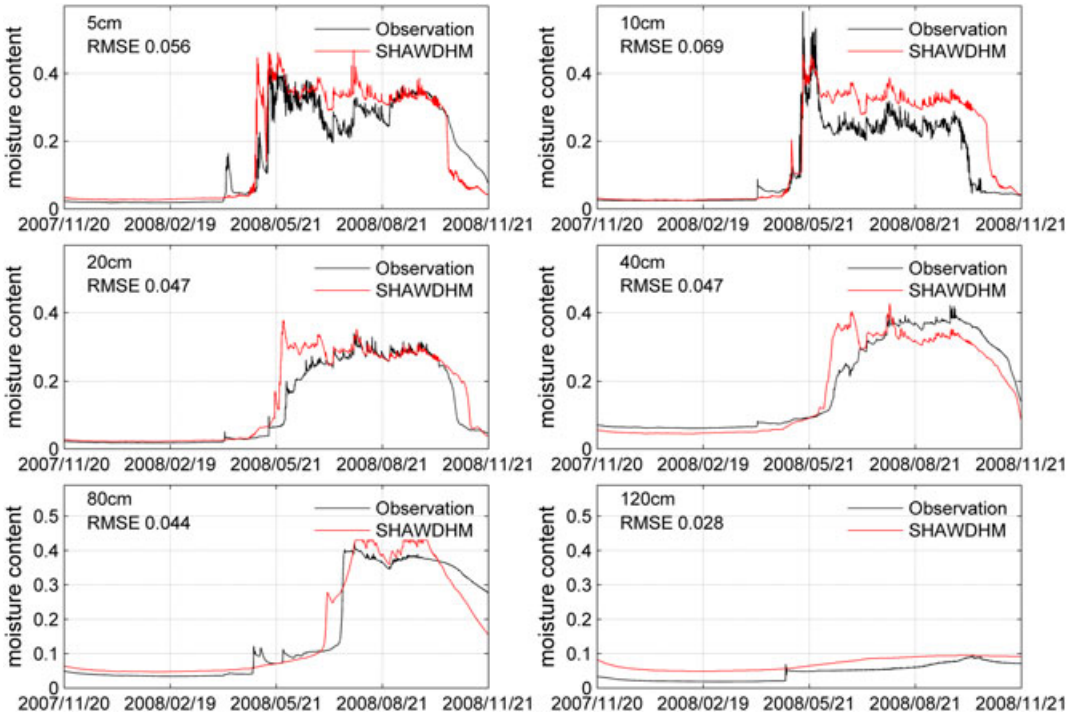

Figure 12. Hourly observed and simulated volumetric liquid soil water content at several depths at DY from 21 November 2007 to 20 November 2008

process was constrained to the first 15 cm below the surface; deeper soil remained frozen. Snowmelt from the surface was perched above the thawing front because of the impermeable underlying frozen soil. This explained the observed peak of liquid water content at 10 cm. However, the simulated peak value was lower because the corresponding simulated soil thawing depth was a little deeper (Figure 7). Perched water in the model was not as significant as the measurement. When frozen soil thawed downward, the perched water infiltrated rapidly, and the soil water content decreased. The model captured the pattern of liquid soil water content, although some discrepancy occurred between the simulated and observed values. This result is expected because the complexities of actual conditions cannot be fully modelled, particularly in mountainous areas with high heterogeneity in soil properties, vegetation structure, and topography.

Stream discharge

A stream flow gauge was installed at BG in 2008. The stream flow rate was measured hourly during the initial stage of hydrography to determine the timing of diurnal maximum and minimum. The flow rate was then measured at least three times daily. The average daily discharge was aggregated from measurement and was compared with simulated values during the period from 17 January 2008 to 20 November 2008, as shown in Figure 13. Figure 14 compares hourly simulated discharge with observed values.

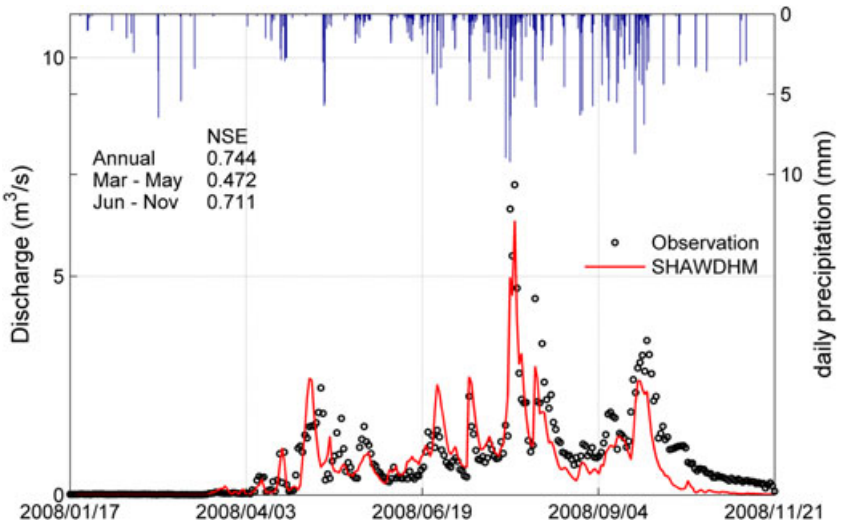

Figure 13. Daily simulated and observed discharge

DOI: 10.1002/hyp

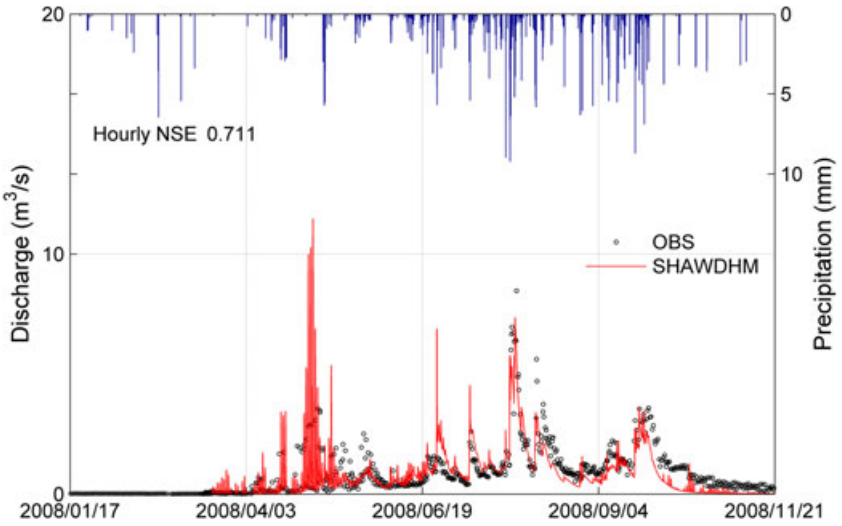

Figure 14. Hourly simulated and observed discharge

Snow began to melt in March from the lower regions of the watershed. Because the melting extent was limited, the runoff was initially small. As the air temperature increased in April, the snowmelt extended rapidly toward upper slope regions (upper right-hand panel in Figure 5); meanwhile, only surface soil thawed in the watershed (Figure 7). The underlying frozen soil prohibited snowmelt from infiltrating downward. Therefore, the snowmelt runoff was greatly enhanced, and the peak discharge was even higher than that in summer (Yang *et al.*, 1993). In addition, the snowmelt runoff showed high diurnal variation because the heat source for melting was higher in the daytime and lower at night.

As shown in Figures 13 and 14, the diurnal peak values of simulated discharge from April to May were higher than those observed, whereas the simulated daily discharge was in good agreement with the measurement. NSE of daily discharge from March to May was 0.472. The peak discharge in mid-August was underestimated. The discharge in fall and winter was generally smaller than observation. Although the watershed is small, precipitation varies in mountainous areas owing to orographic effects. Errors may be introduced when uniformly distributed precipitation is assumed, which may explain the underestimated discharge. In addition, continuous light snowfall was ignored as noise because the method used to derive precipitation from snow depth was based on a threshold of 2 cm. Another important factor is that the baseflow is complicated in the watershed. The method used in the model was not sufficient to depict the baseflow in such mountainous areas subject to both seasonal frozen soil and permafrost. Moreover, errors in soil temperature simulation could also lead to discharge underestimation in fall and winter. As shown in the top panels of Figure 10, measurements indicated that the surface soil at 5 and 10 cm began to refreeze in September, which would prohibit snowmelt and rainfall from infiltrating, thus enhancing the surface runoff. In contrast, the corresponding simulated soil temperatures remained positive for a lengthy period.

Overall, the simulated discharge agreed well with observations. NSE of the daily hydrograph was 0.744 in the entire simulation period and 0.711 from June to November. NSE of the hourly discharge was 0.711. Figure 15(a) presents a scatter plot of observed discharge versus corresponding simulated values; the

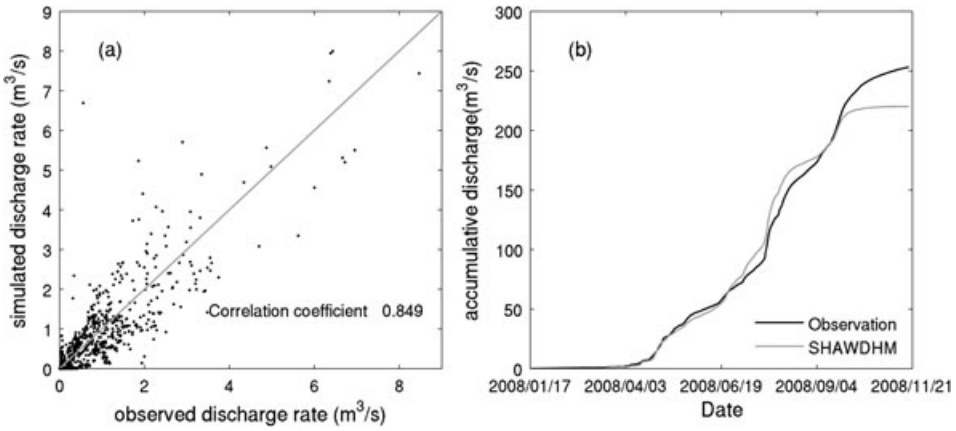

Figure 15. a) Comparison of hourly simulated and observed discharge rates; b) comparison of cumulative curves of simulated and observed daily discharge rates

DOI: 10.1002/hyp

correlation coefficient was 0.849. Figure 15(b) presents cumulative curves of simulated and observed daily discharge. Inspection of the curves shows that the model performance was acceptable in spring and early summer. The model underestimated discharge in fall and winter. The total runoff was underestimated by approximately 13%.

Water balance

The total precipitation was approximately 703 mm in the watershed during the entire simulation period. The simulated evapotranspiration of 296 mm is slightly larger than the average annual value of 238 mm estimated by Yang *et al*. (1993), which was calculated according to a water balance analysis by using observations of steam runoff and precipitation from 1984 to 1991. According to the model, the runoff depth of the watershed was approximately 488.4 mm, and the water storages of soil, groundwater system, and snow cover were decreased by 34.5 mm, 38.8 mm (average soil water content decreased from 0.384 to 0.352), and 5.7 mm, respectively. In any time step, the surface runoff from all model grids was summed as the total surface runoff at the watershed outlet without consideration of river routing. The total subsurface flow and baseflow could be estimated in the same manner. The subsurface flow accounted for approximately 69.6% of the total runoff, while the surface flow and baseflow accounted for 14.1% and 16%, respectively. As shown in Figure 16, surface runoff mainly occurred in the snowmelt season with shallow underlying frozen soil. In other seasons with deep frozen soil, surface runoff rarely occurred, even in summer with extensive precipitation.

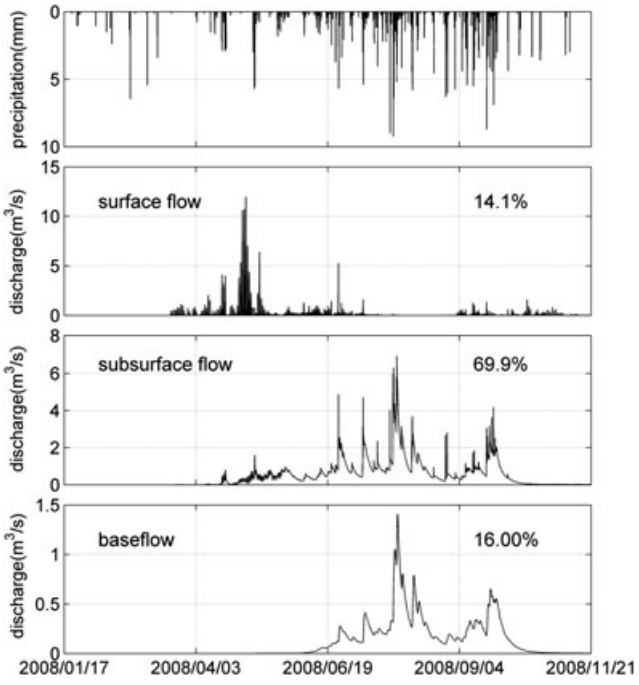

Figure 16. Hydrograph separation according to the combined model

CONCLUSIONS

Snow and frozen soil prevail in cold regions worldwide, and their effects on hydrological processes and water resources remain research focuses in the context of global climate change. In this study, the SHAW and GBHM models were fully coupled, and the combined model assimilated advantages from both components. The model simultaneously simulated the vertical and lateral water transfer as well as the vertical heat fluxes on hillslopes and considered the effects of frozen soil and snowmelt on hydrological cycles on a watershed scale. In addition, the heat and water fluxes were described in a physically based manner and region-specific empirical parameters were eliminated; however, the model required additional spatially distributed inputs.

The model was evaluated in the Binggou watershed, a small mountainous watershed in a cold region, and the results were compared with *in situ* observations. The simulated soil temperature, liquid soil water content, and snow depth were highly consistent with field observations. Although no spatially distributed observations were available to evaluate simulated soil freezing, thawing, and snow depth in the watershed, their spatial temporal changes were reasonable and in compliance with facts. The permafrost region determined by the model was in good agreement with the survey reported by Yang *et al*. (1993). The model showed good performance in simulating soil freezing/thawing and snow accumulation/melting. Both frozen soil and snow played important roles in stream discharge. Because the simulated snowmelt and frost table were reasonable, the discharge prediction was accurate in spring and early summer. However, peak runoff in summer and discharge in fall and winter were underestimated. The cumulative simulated runoff was approximately 13% smaller than that measured. According to the model, surface runoff in the watershed mainly occurred in snowmelt season with shallow underlying frozen soil. These results prove that the coupling strategy is reasonable, and the combined model is practical for cold regions.

Frozen soil, snowmelt, groundwater, and other processes are correlated in cold regions. To assess the impacts of global warming on hydrological cycles and water resources in such environments, these components should be properly integrated. The absence or erroneous representation of one process in the modelling system would result in errors in other processes. In mountainous areas subject to both seasonal frozen soil and permafrost, the groundwater flow is complicated. However, the influences of frozen soil on groundwater flow were resolved in a simple and rough manner. Lateral groundwater interaction between the model grids was also ignored in the model. A more robust groundwater flow module should be incorporated to improve the baseflow prediction. In addition, uncertainties from inputs account for a large part of uncertainties in the simulation. To better understand the hydrological processes in cold regions, an integrated watershed observation system is critical (Li *et al*., 2009b), particularly in mountainous regions. Retrievals of distributed forcing data, state

DOI: 10.1002/hyp

variables of the land surface system, and relevant model parameters such as soil and vegetation together form the cornerstone of watershed scale model development, improvement, and verification.

ACKNOWLEDGEMENTS

The authors thank Professor Des Walling and the referees for the suggestions and critical comments. This work is supported by the National Science Fund for Distinguished Young Scientists, 'Development of a Catchment-Scale Land Data Assimilation System' (grant number: 40925004), the project 'Land Surface Modelling and Data Assimilation Research' (grant number: 2009AA122104) from the National High Technology Research and Development Program (863) of China, the Knowledge Innovation Program of the Chinese Academy of Sciences (CAS) (grant number: KZCX2-EW-312), and the Foundation for Young Talents in Cold and Arid Regions Environmental and Engineering Research Institute of CAS (grant number: Y251A81).

REFERENCES

Bayard D, Stahli M. 2005. Effects of frozen soil on the groundwater recharge in alpine areas. In *Climate and hydrology in mountain areas*, de Jong C, Collins DN, Ranzi R (eds). Wiley; 73–83. doi: 10.1002/0470858249.ch7.

Bayard D, Stahli M, Parriaux A, Fluhler H. 2005. The influence of seasonally frozen soil on the snowmelt runoff at two Alpine sites in southern Switzerland. *Journal of Hydrology* **309**: 66–84. doi: 10.1016/j.jhydrol.2004.11.012.

Chen RS, Lu SH, Kang ES, Ji XB, Zhang Z, Yang Y, Qing WW. 2008. A distributed water-heat coupled model for mountainous watershed of an inland river basin of Northwest China (I) model structure and equations. *Environmental Geology* **53**: 1299–1309. doi: 10.1007/s00254-007-0738-2.

Cherkauer KA, Lettenmaier DP. 1999. Hydrologic effects of frozen soils in the upper Mississippi River basin. *Journal of Geophysical Research* **104**: 19599–19610. doi:10.1029/1999JD900337.

Cherkauer KA, Lettenmaier DP. 2003. Simulation of spatial variability in snow and frozen soil. *Journal of Geophysical Research-Atmospheres* **108**: 8858. doi: 10.1029/2003JD003575.

Clapp RB, Hornberger GM. 1978. Empirical Equations for Some Soil Hydraulic-Properties. *Water Resources Research* **14**: 601–604. doi: 10.1029/WR014i004p00601.

Flerchinger G. 2000. *The simultaneous heat and water (SHAW) model: user's manual*. Technical Rep: NWRC **10**.

Flerchinger G, Saxton K. 1989. Simultaneous heat and water model of a freezing snow-residue-soil system I. Theory and development. *Transactions of ASAE* **32**: 565–571.

Fuchs M, Campbell GS, Papendick RI. 1978. Analysis of Sensible and Latent Heat-Flow in a Partially Frozen Unsaturated Soil. *Soil Science Society of America Journal* **42**: 379–385.

Green WH, Ampt G. 1911. Studies on soil physics, 1. The flow of air and water through soils. *J. Agricultural Sciences* **4**: 1–24.

Hall RL, Huntingford C, Harding RJ, Lloyd CR, Cox PM. 2003. An improved description of soil hydraulic and thermal properties of arctic peatland for use in a GCM. *Hydrological Processes* **17**: 2611–2628. doi: 10.1002/hyp.1265.

Harlan R. 1973. Analysis of coupled heat-fluid transport in partially frozen soil. *Water Resources Research* **9**: 1314–1323. doi: 10.1029/WR009i005p01314.

Hayashi M, Goeller N, Quinton WL, Wright N. 2007. A simple heat-conduction method for simulating the frost-table depth in hydrological models. *Hydrological Processes* **21**: 2610–2622. doi: 10.1002/hyp.6792.

Hedstrom NR, Pomeroy JW. 1998. Measurements and modelling of snow interception in the boreal forest. *Hydrological Processes* **12**: 1611–1625. doi: 10.1002/(SICI)1099-1085(199808/09).

Hirota T, Pomeroy JW, Granger RJ, Maule CP. 2002. An extension of the force-restore method to estimating soil temperature at depth and evaluation for frozen soils under snow. *Journal of Geophysical Research-Atmospheres* **107**. doi: 10.1029/2001jd001280.

Jansson P, Halldin S. 1979. Model for the annual water and heat flow in a layered soil. *Comparison of Forest and Energy Exchange Models. International Society for microbial Ecology Copenhagen* 145–163. doi: 10.1016/0167-8809(87)90099-5.

Jansson PE, Moon DS. 2001. A coupled model of water, heat and mass transfer using object orientation to improve flexibility and functionality. *Environmental Modelling & Software* **16**: 37–46. doi: 10.1016/S1364-8152(00)00062-1.

Jaranilla-Sanchez PA, Wang L, Koike T. 2011. Modeling the hydrologic responses of the Pampanga River basin, Philippines: A quantitative approach for identifying droughts. *Water Resources Research* **47**: W03514. doi: 10.1029/2010wr009702.

Konrad JM, Duquennoi C. 1993. A Model for Water Transport and Ice Lensing in Freezing Soils. *Water Resources Research* **29**: 3109–3124. doi: 10.1029/93WR00773.

Koren V. 2006. Parameterization of frozen ground effects: sensitivity to soil properties. *Predictions in Ungauged Basins: Promise and Progress* **303**: 125–133.

Koren V, Schaake J, Mitchell K, Duan QY, Chen F, Baker J. 1999. A parameterization of snowpack and frozen ground intended for NCEP weather and climate models. *Journal of Geophysical Research* **104**: 19569–19585. doi: 10.1029/1999JD900232.

Li HY, Wang J. 2011. Simulation of snow distribution and melt under cloudy conditions in an Alpine watershed. *Hydrology and Earth System Sciences* **15**: 2195–2203. doi: 10.5194/hess-15-2195-2011.

Li Q, Sun S, Xue Y. 2010. Analyses and development of a hierarchy of frozen soil models for cold region study. *Journal of Geophysical Research* **115**: D03107. doi: 10.1029/2009JD012530.

Li Q, Sun SF, Dai QD. 2009a. The Numerical Scheme Development of a Simplified Frozen Soil Model. *Advances in Atmospheric Sciences* **26**: 940–950. doi: 10.1007/s00376-009-7174-z.

Li X, Cheng GD, Jin HJ, Kang E, Che T, Jin R, Wu LZ, Nan ZT, Wang J, Shen YP. 2008. Cryospheric change in China. *Global and Planetary Change* **62**: 210–218. DOI 10.1016/j.gloplacha.2008.02.001.

Li X, Koike T. 2003. Frozen soil parameterization in SiB2 and its validation with GAME-Tibet observations. *Cold Regions Science and Technology* **36**: 165–182. doi: 10.1016/S0165-232X(03)00009-0.

Li X, Li XW, Li ZY, Ma MG, Wang J, Xiao Q, Liu Q, Che T, Chen EX, Yan GJ. 2009b. Watershed allied telemetry experimental research. *Journal of Geophysical Research* **114**: D22103. doi: 10.1029/2008jd011590.

Liang X, Lettenmaier DP, Wood EF, Burges SJ. 1994. A Simple Hydrologically Based Model of Land-Surface Water and Energy Fluxes for General-Circulation Models. *Journal of Geophysical Research-Atmospheres* **99**: 14415–14428. doi: 10.1029/94JD00483.

Lundin LC. 1990. Hydraulic properties in an operational model of frozen soil. *Journal of Hydrology* **118**: 289–310. doi: 10.1016/0022-1694(90)90264-X.

Luo LF, Robock A, Vinnikov KY, Schlosser CA, Slater AG, Boone A, Braden H, Cox P, de Rosnay P, Dickinson RE, Dai YJ, Duan QY, Etchevers P, Henderson-Sellers A, Gedney N, Gusev YM, Habets F, Kim JW, Kowalczyk E, Mitchell K, Nasonova ON, Noilhan J, Pitman AJ, Schaake J, Shmakin AB, Smirnova TG, Wetzel P, Xue YK, Yang ZL, Zeng QC. 2003. Effects of frozen soil on soil temperature, spring infiltration, and runoff: Results from the PILPS 2(d) experiment at Valdai, Russia. *Journal of Hydrometeorology* **4**: 334–351. doi: 10.1175/1525-7541(2003)4 < 334:EOFSOS > 2.0.CO;2.

Niu GY, Yang ZL. 2006. Effects of frozen soil on snowmelt runoff and soil water storage at a continental scale. *Journal of Hydrometeorology* **7**: 937–952. doi: 10.1175/JHM538.1.

Nyberg L, Stahli M, Mellander PE, Bishop KH. 2001. Soil frost effects on soil water and runoff dynamics along a boreal forest transect: 1. Field investigations. *Hydrological Processes* **15**: 909–926. doi: 10.1002/hyp.256.

Pfafstetter O. 1989. Classification of hydrographic basins: coding methodology. *unpublished manuscript, Departamento Nacional de Obras de Saneamento, August* **18**: 1–2.

Pohl S, Davison B, Marsh P, Pietroniro A. 2005. Modelling spatially distributed snowmelt and meltwater runoff in a small Arctic catchment with a hydrology land-surface scheme (WATCLASS). *Atmosphere-Ocean* **43**: 193–211. doi: 10.3137/ao.430301.

Pomeroy JW, Gray DM, Brown T, Hedstrom NR, Quinton WL, Granger RJ, Carey SK. 2007. The cold regions hydrological process representation and model: a platform for basing model structure on physical evidence. *Hydrological Processes* **21**: 2650–2667. doi: 10.1002/Hyp.6787.

Pomeroy JW, Gray DM, Shook KR, Toth B, Essery RLH, Pietroniro A, Hedstrom N. 1998. An evaluation of snow accumulation and ablation processes for land surface modelling. *Hydrological Processes* **12**: 2339–2367. doi: 10.1002/(sici)1099-1085(199812)12:15 < 2339::aid-hyp800 > 3.0.co;2-l.

Quinton WL, Carey SK. 2008. Towards an energy-based runoff generation theory for tundra landscapes. *Hydrological Processes* **22**: 4649–4653. doi: 10.1002/hyp.7164.

Rawlins MA, Lammers RB, Frolking S, Fekete BM, Vorosmarty CJ. 2003. Simulating pan-Arctic runoff with a macro-scale terrestrial water balance model. *Hydrological Processes* **17**: 2521–2539. doi: 10.1002/hyp.1271.

Rigon R, Bertoldi G, Over TM. 2006. GEOtop: A distributed hydrological model with coupled water and energy budgets. *Journal of Hydrometeorology* **7**: 371–388. doi: 10.1175/JHM497.1.

Saxton KE, Rawls WJ. 2006. Soil water characteristic estimates by texture and organic matter for hydrologic solutions. *Soil Science Society of America Journal* **70**: 1569–1578. doi: 10.2136/sssaj2005.0117.

Schmidt R, Gluns DR. 1991. Snowfall interception on branches of three conifer species. *Canadian Journal of Forest Research* **21**: 1262–1269. doi: 10.1139/x91-176.

Shi X, Yu D, Warner E, Pan X, Petersen G, Gong Z, Weindorf D. 2004. Soil database of 1: 1,000,000 digital soil survey and reference system of the Chinese genetic soil classification system. *Soil Survey Horizons* **45**: 129–136.

Slater AG, Schlosser CA, Desborough CE, Pitman AJ, Henderson-Sellers A, Robock A, Vinnikov KY, Mitchell K, Boone A, Braden H, Chen F, Cox PM, de Rosnay P, Dickinson RE, Dai YJ, Duan Q, Entin J, Etchevers P, Gedney N, Gusev YM, Habets F, Kim J, Koren V, Kowalczyk EA, Nasonova ON, Noilhan J, Schaake S, Shmakin AB, Smirnova TG, Verseghy D, Wetzel P, Yue X, Yang ZL, Zeng Q. 2001. The representation of snow in land surface schemes: Results from PILPS 2(d). *Journal of Hydrometeorology* **2**: 7–25. doi: 10.1175/1525-7541(2001)002 < 0007:TROSIL > 2.0.CO;2.

Stahli M, Jansson PE, Lundin LC. 1996. Preferential water flow in a frozen soil - A two-domain model approach. *Hydrological Processes* **10**: 1305–1316. doi: 10.1002/(sici)1099-1085(199610)10:10 < 1305::aid-hyp462 > 3.0.co;2-f.

Stahli M, Jansson PE, Lundin LC. 1999. Soil moisture redistribution and infiltration in frozen sandy soils. *Water Resources Research* **35**: 95–103. doi: 10.1029/1998WR900045.

Stahli M, Nyberg L, Mellander PE, Jansson PE, Bishop KH. 2001. Soil frost effects on soil water and runoff dynamics along a boreal transect: 2.Simulations. *Hydrological Processes* **15**: 927–941. doi: 10.1002/hyp.232.

Takata K. 2002. Sensitivity of land surface processes to frozen soil permeability and surface water storage. *Hydrological Processes* **16**: 2155–2172. doi: 10.1002/hyp.1148.

Verdin K, Verdin J. 1999. A topological system for delineation and codification of the Earth's river basins. *Journal of Hydrology* **218**: 1–12. doi: 10.1016/S0022-1694(99)00011-6.

Wang L, Koike T, Yang K, Jackson TJ, Bindlish R, Yang DW. 2009a. Development of a distributed biosphere hydrological model and its evaluation with the Southern Great Plains Experiments (SGP97 and SGP99). *Journal of Geophysical Research-Atmospheres* **114**. doi: 10.1029/2008jd010800.

Wang L, Koike T, Yang K, Jin R, Li H. 2010. Frozen soil parameterization in a distributed biosphere hydrological model. *Hydrology and Earth System Sciences* **14**: 557–571. doi: 10.5194/hess-14-557-2010.

Wang L, Koike T, Yang K, Yeh PJF. 2009b. Assessment of a distributed biosphere hydrological model against streamflow and MODIS land surface temperature in the upper Tone River Basin. *Journal of Hydrology* **377**: 21–34. doi: 10.1016/j.jhydrol.2009.08.005.

Woo MK, Arain MA, Mollinga M, Yi S. 2004. A two-directional freeze and thaw algorithm for hydrologic and land surface modelling. *Geophysical Research Letters* **31**: L12501. doi: 10.1029/2004GL019475.

Woo MK, Kane DL, Carey SK, Yang DQ. 2008. Progress in permafrost hydrology in the new millennium. *Permafrost and Periglacial Processes* **19**: 237–254. doi: 10.1002/ppp.613.

Wright N, Quinton WL, Hayashi M. 2008. Hillslope runoff from an ice-cored peat plateau in a discontinuous permafrost basin, Northwest Territories, Canada. *Hydrological Processes* **22**: 2816–2828. doi: 10.1002/hyp.7005.

Yamazaki Y, Kubota J, Ohata T, Vuglinsky V, Mizuyama T. 2006. Seasonal changes in runoff characteristics on a permafrost watershed in the southern mountainous region of eastern Siberia. *Hydrological Processes* **20**: 453–467. doi: 10.1002/hyp.5914.

Yang D. 1998. *Distributed hydrologic model using hill-slope discritization based on catchment area function: development and application*. University of Tokyo: Japan.

Yang D, Herath S, Musiake K. 2002. A hillslope-based hydrological model using catchment area and width functions. *Hydrological Sciences Journal* **47**: 49–65. doi: 10.1002/hyp.5752.

Yang D, Koike T, Tanizawa H. 2004. Application of a distributed hydrological model and weather radar observations for flood management in the upper Tone River of Japan. *Hydrological Processes* **18**: 3119–3132. doi: 10.1002/hyp.5752.

Yang Z, Yang Z, Liang F, Wang Q. 1993. Permafrost hydrological processes in Binggou basin of Qilian mountains. *Journal of Glaciology and Geocryology* **15**(2): 235–241. (in chinese)

Yi S, Arain MA, Woo MK. 2006. Modifications of a land surface scheme for improved simulation of ground freeze-thaw in northern environments. *Geophysical Research Letters* **33**: L13501. doi: 10.1029/2006GL026340.

Zhang T, Barry RG, Knowles K, Heginbottom JA, Brown J. 1999. Statistics and characteristics of permafrost and ground-ice distribution in the Northern Hemisphere. *Polar Geography* **23**: 132–154. doi: 10.1080/10889379909377670.

Zhang T, Barry RG, Knowles K, Ling F, Armstrong RL. 2003a. *Distribution of seasonally and perenially frozen ground in the Northern Hemisphere, Proceedings of the 8th International Conference on Permafrost*, Phillips M, Springman SM, Arenson LU (eds). A. A. Balkema: PublishersZurich, Switzerland, July 21–25, 2003, Vol. **2**, 1289–1294.

Zhang YS, Ohata T, Ersi K, Yao TD. 2003b. Observation and estimation of evaporation from the ground surface of the cryosphere in eastern Asia. *Hydrological Processes* **17**: 1135–1147. doi: 10.1002/hyp.1183.

Zhang Z, Kane DL, Hinzman LD. 2000. Development and application of a spatially-distributed Arctic hydrological and thermal process model (ARHYTHM). *Hydrological Processes* **14**: 1017–1044. doi: 10.1002/(SICI)1099-1085(20000430)14:6 < 1017::AID-HYP982 > 3.0.CO;2-G.